

SHORT TITLE

TITLE

By

IAN D. ROBERTS, B.Sc.

A Thesis

Submitted to the School of Graduate Studies

in Partial Fulfilment of the Requirements

for the Degree

Master of Science

McMaster University

©Copyright by Ian Roberts, Submission Month 2016

MASTER OF SCIENCE (2016)

McMaster University

(Physics and Astronomy)

Hamilton, Ontario

TITLE: Title

AUTHOR: Ian Roberts, B.Sc. (McMaster University)

SUPERVISORS: Laura Parker

NUMBER OF PAGES: xi, 48

Abstract

Abstract...

Acknowledgements

Acknowledgements here

dedication here

Table of Contents

Descriptive Notes	ii
Abstract	iii
Acknowledgements	iv
List of Figures	viii
List of Tables	xi
Chapter 1 Introduction	1
Chapter 2 Mass segregation trends in SDSS galaxy groups	3
2.1 Introduction	3
2.2 Data	6
2.3 Results	9
2.3.1 Mass segregation in SDSS groups	9
2.3.2 Massive galaxy fraction	10
2.4 Discussion	12
2.4.1 Effect of including low-mass galaxies	12
2.4.2 Halo mass dependence	13
2.4.3 Reconciling previous results	15
2.5 Conclusion	15
2.6 Acknowledgements	16

Chapter 3	Comparing galaxy morphology and star formation properties in X-ray bright and faint groups and cluster	23
3.1	Introduction	23
3.2	Data	27
3.2.1	Yang group catalogue	27
3.2.2	SDSS X-ray catalogue	29
3.2.3	Final data set	30
3.3	Results	35
3.3.1	Star-forming and morphology trends in strong and weak L_X samples	35
3.3.2	Radial dependence of star-forming and morphology trends	36
3.4	Discussion	38
3.5	Summary & Conclusions	38

List of Figures

2.1	All panels show mean mass as a function of normalized distance for various halo mass bins, with error bars corresponding to 1σ statistical errors. The solid lines correspond to weighted least-squares fits for each halo mass bin. Top left: unweighted sample, for galaxies with $\log(M_{\text{star}}/M_{\odot}) > 10.5$. Top right: unweighted sample, for galaxies with $\log(M_{\text{star}}/M_{\odot}) > 10.0$. Bottom left: V_{max} -weighted sample, for galaxies with $\log(M_{\text{star}}/M_{\odot}) > 9.0$. Bottom right: V_{max} -weighted sample, for galaxies with $\log(M_{\text{star}}/M_{\odot}) > 8.5$. Note that different mass scales are used in each panel. There are more halo mass bins in the bottom row due to the increased number of low-mass galaxies as a result of V_{max} weighting.	9
2.2	Fraction of massive galaxies with respect to normalized radial distance. Error bars are given by a 1σ binomial confidence interval, calculated using the beta distribution as outlined in Cameron (2011). The solid lines correspond to weighted least-squares fits for each halo mass bin. Left-hand panel: the fraction of galaxies with $\log(M_{\text{star}}/M_{\odot}) > 10.25$ as a function of radial distance, for the unweighted sample with $M_{\text{star}} > 10^{10}M_{\odot}$. Right-hand panel: the fraction of galaxies with $\log(M_{\text{star}}/M_{\odot}) > 10.5$ as a function of radial distance, for the unweighted sample with $M_{\text{star}} > 10^{10}M_{\odot}$.	11

3.1	Density contours for log X-ray luminosity versus log halo mass. Dashed line corresponds to the linear least-squares best-fitting relationship.	31
3.2	Smoothed distributions for halo mass and X-ray luminosity within the sample. Distributions are shown for both the X-ray strong (red, dashed) and the X-ray weak (blue, solid) samples. Shaded regions correspond to 2σ confidence intervals obtained from ran- dom bootstrap resampling.	39
3.3	Left: star-forming fraction versus stellar mass for the four X-ray lu- minosity quartiles of the data sample. Right: disc fraction versus stellar mass for the four X-ray luminosity quartiles of the sam- ple. Error bars correspond to 1σ Bayesian binomial confidence intervals given in Cameron (2011)	40
3.4	Star-forming (solid lines) and disc (dashed lines) fractions versus stellar mass, for different halo mass bins and the XRW (blue) and XRS (red) samples. Error bars correspond to 1σ Bayesian binomial confidence intervals given in Cameron (2011)	41
3.5	Star-forming (solid lines) and disc (dashed lines) fractions versus stellar mass, for galaxies outside of their host X-ray radius and for different halo mass bins and the two L_X samples. Error bars correspond to 1σ Bayesian binomial confidence intervals given in Cameron (2011)	42
3.6	Same as Fig. 3.5 for galaxies inside of their host X-ray radius. . .	43

3.7	SF and disc excess versus stellar mass for both galaxies within (purple, solid) and outside (green, dashed) of the X-ray radius. Panels a-d show SF excess for four halo mass bins and panels e-h show disc excess for four halo mass bins. Shaded regions represent 1σ confidence intervals.	43
-----	--	----

List of Tables

Chapter 1

Introduction

Chapter 2

Mass segregation trends in SDSS galaxy groups

2.1 Introduction

It has been well established that galaxy properties depend strongly on local environment (e.g. Oemler, 1974; Hogg et al., 2004; Blanton et al., 2005a; Tal et al., 2014). Galaxies in dense environments such as clusters tend to have lower star formation rates (SFRs), while isolated field galaxies are generally actively forming stars (e.g. Balogh et al., 2000; Ball et al., 2008; Wetzel et al., 2012). It is also well known that galaxy properties, such as SFR, depend strongly on galaxy mass (e.g. Poggianti et al., 2008). It is critical to study the distribution of galaxy masses within haloes of different masses in order to ascertain whether the variations in galaxy properties with environment are due to physical mechanisms acting in dense environments, or simply due to the fact that high-density environments contain more high-mass galaxies. Intermediate-density environments, galaxy groups, represent not only the most common environment in the local Universe (Geller & Huchra, 1983; Eke

et al., 2005), but also represent the environment where many physical processes are efficient. Galaxy interactions such as mergers and harassment are favoured in this environment because of the low relative velocities between galaxies (Zabludoff & Mulchaey, 1998; Brough et al., 2006).

The study of mass segregation in groups can be used to elucidate information on physical processes such as dynamical friction, galaxy mergers, and tidal stripping. Mass segregation in bound structures has generally been predicted as a result of dynamical friction (Chandrasekhar, 1943). Dynamical friction acts as a drag force on orbiting bodies and massive galaxies within groups and clusters are expected to migrate to smaller radii as time progresses. If dynamical friction is a dominant factor, then clear mass segregation should be observed in evolved groups and clusters.

Galaxy groups are not static systems, but are constantly being replenished by infalling galaxies from the field. Infalling galaxies are preferentially found at large radii (Wetzel et al., 2013) and the difference in stellar mass distributions between evolved group members and infalling galaxies could affect the strength of mass segregation.

If significant mass segregation is not found, then this implies that either: the time-scale associated with dynamical friction is greater than the age of the group/cluster, or that there are other physical processes, such as merging, tidal stripping, or pre-processing, which are playing a more important role than dynamical friction.

Recent work has shown conflicting results with regards to the presence of mass segregation in groups and clusters. Ziparo et al. (2013) find no evidence

for strong mass segregation in X-ray selected groups out to $z = 1.6$, for a sample of galaxies with $M_{\text{star}} > 10^{10.3}M_{\odot}$. von der Linden et al. (2010) examine Sloan Digital Sky Survey (SDSS) galaxy clusters and find no evidence for mass segregation in four different redshift bins at $z < 0.1$. von der Linden et al. make redshift-dependent stellar mass cuts ranging from $10^{9.6}$ to $10^{10.5}M_{\odot}$. Vulcani et al. (2013) use mass-limited samples at $0.3 \leq z \leq 0.8$ from the IMACS Cluster Building Survey and the ESO Distant Cluster Survey, with stellar mass cuts at $M_{\text{star}} > 10^{10.5}M_{\odot}$ and $M_{\text{star}} > 10^{10.2}M_{\odot}$, respectively, to study galaxy stellar mass functions in different environments. Vulcani et al. find no statistical differences between mass functions of galaxies located at different cluster-centric distances.

Conversely, Balogh et al. (2014) find evidence for mass segregation in Group Environment Evolution Collaboration 2 (GEEC2) groups at $0.8 < z < 1$, using as stellar-mass-limited sample with $M_{\text{star}} > 10^{10.3}M_{\odot}$. Using a volume limited sample of zCOSMOS groups, Presotto et al. (2012) find evidence for mass segregation in their whole sample at both $0.2 \leq z \leq 0.45$ and $0.45 \leq z \leq 0.8$. Presotto et al. also break their sample into rich and poor groups at $0.2 \leq z \leq 0.45$, and find evidence for mass segregation within rich groups but find no evidence for mass segregation within poor groups. Using a V_{max} -weighted sample with a stellar mass cut at $10^{9.0}M_{\odot}$, van den Bosch et al. (2008) find evidence for mass segregation in SDSS groups.

It is clear that there is no consensus regarding the strength of mass segregation in groups and clusters or its halo mass dependence.

In this Letter, we present evidence of the presense of a small, but significant, amount of mass segregation in SDSS galaxy groups. We show that the detection of mass segregation is dependent on stellar mass completeness, with completeness cuts at relatively high stellar masses potentially masking underlying mass segregation trends. We also show that the strength of mass segregation scales inversely with halo mass, with cluster-sized haloes showing little to no observable mass segregation. In Section 2.2, we briefly describe our data set, in Section 2.3 we present our results from this work, in Section ... we provide a discussion of our results, and in Section ... we give a summary of the results and make concluding statements.

In this Letter, we assume a flat Λ cold dark matter cosmology with $\Omega_M = 0.3$, $\Omega_\Lambda = 0.7$, and $H_0 = 70 \text{ km s}^{-1} \text{ Mpc}^{-1}$.

2.2 Data

The results presented in this Letter utilize the group catalogue of Yang et al. (2007). This catalogue is constructed by applying the halo-based group finder of Yang et al. (2005, 2007) to the New York University Value-Added Galaxy Catalogue (NYU-VAGC; Blanton et al. 2005b), which is based on the SDSS Data Release 7 (DR7; Abazajian et al. 2009). Stellar masses are obtained from the NYU-VAGC and are computed using the methodology of Blanton & Roweis (2007), assuming a Chabrier (2003) initial mass function. Halo masses are determined using the ranking of the characteristic stellar mass, $M_{\star, \text{grp}}$, and assuming a relationship between M_{halo} and $M_{\star, \text{grp}}$ (Yang et al., 2007). $M_{\star, \text{grp}}$ is defined by Yang et al. as

$$M_{\star,\text{grp}} = \frac{1}{g(L_{19.5}, L_{\text{lim}})} \sum_i \frac{M_{\text{star},i}}{C_i}, \quad (2.1)$$

where $M_{\text{star},i}$ is the stellar mass of the i th member galaxy, C_i is the completeness of the survey at the position of that galaxy, and $g(L_{19.5}, L_{\text{lim}})$ is a correction factor which accounts for galaxies missed due to the magnitude limit of the survey.

Halo-centric distance for each galaxy is not given explicitly in the Yang catalogue; however, we calculate it using the redshift of the group and the angular separation of the galaxy and halo centre on the sky. We measure group-centric radius from the luminosity-weighted centre of each group, and normalize our group-centric radii by R_{200} . We use the definition for R_{200} as given in Carlberg et al. (1997)

$$R_{200} = \frac{\sqrt{3}\sigma}{10H(z)}, \quad (2.2)$$

where the Hubble parameter, $H(z)$, is defined as

$$H(z) = H_0 \sqrt{\Omega_M(1+z)^3 + \Omega_\Lambda}, \quad (2.3)$$

and we calculate the velocity dispersion, σ , as

$$\sigma = 397.9 \text{ km s}^{-1} \left(\frac{M_{\text{halo}}}{10^{14} h^{-1} \text{M}_\odot} \right)^{0.3214}, \quad (2.4)$$

where the above is a fitting function given in Yang et al. (2007).

For our analysis we select group galaxies with redshift, $z < 0.1$, that are within two virial radii of the group centre, and groups with a minimum of three galaxy members – although our results are not sensitive to these specific cuts. For our sample over 95 per cent of group galaxies reside within two virial radii of the group centre. We also subtract the most massive galaxy (MMG) from each group, to ensure that any underlying radial mass trend is not contaminated by the MMG.

This sample is not volume limited, therefore, the sample will suffer from the Malmquist bias. This leads to a bias towards objects of higher luminosity and stellar mass, with increasing redshift. To account for this bias we weight our sample by $1/V_{\text{max}}$, where V_{max} is the comoving volume of the Universe out to a comoving radius at which the galaxy would have met the selection criteria for the sample. For our V_{max} weights we apply the values presented in the catalogue of Simard et al. (2011) to our sample.

In order to investigate the effect of stellar mass limits on the detection of mass segregation, we use samples corresponding to various stellar mass cuts. We perform our analysis on an unweighted sample with two mass cuts corresponding to $M_{\text{star}} > 10^{10.5}M_{\odot}$ (4152 galaxies in 1970 groups) and $M_{\text{star}} > 10^{10.0}M_{\odot}$ (26 774 galaxies in 4534 groups); and a V_{max} -weighted sample with mass cuts at $M_{\text{star}} > 10^{9.0}M_{\odot}$ (56 957 galaxies in 7217 groups) and $M_{\text{star}} > 10^{8.5}M_{\odot}$ (59 791 galaxies in 7289 groups). The unweighted sample is stellar mass complete down to $M_{\text{star}} > 10^{10.0}M_{\odot}$. Therefore, for both the weighted and unweighted sample, we have two different stellar mass cuts, giving us four separate samples in total.

2.3 Results

2.3.1 Mass segregation in SDSS groups

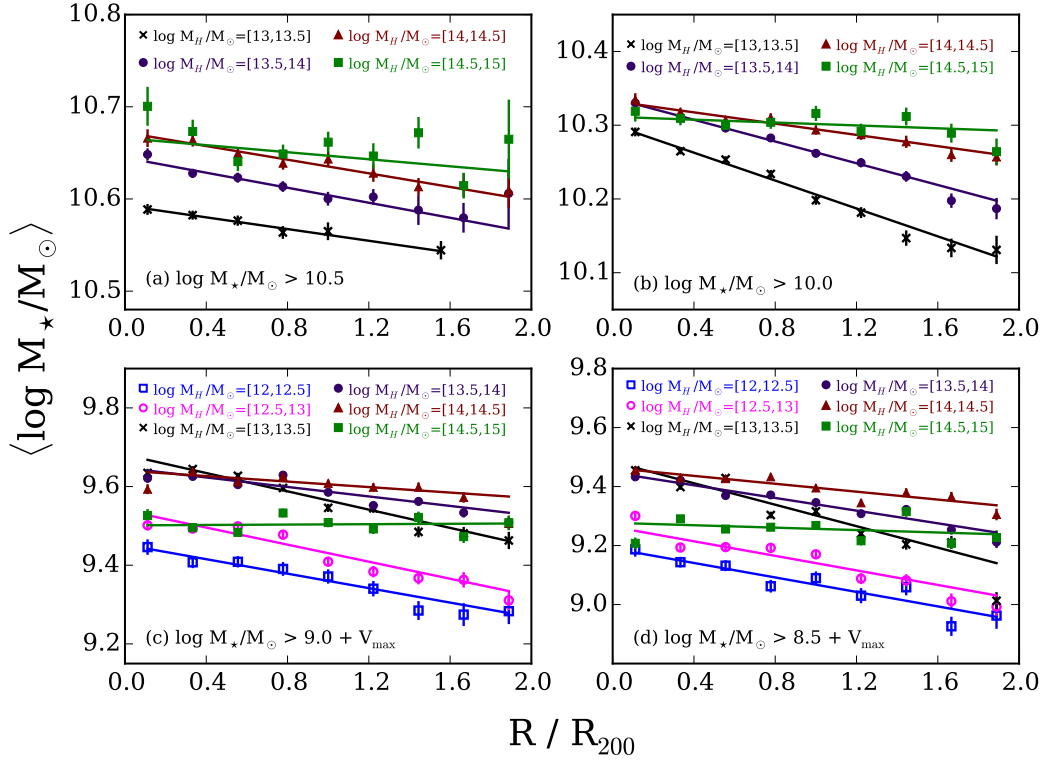


Figure 2.1 All panels show mean mass as a function of normalized distance for various halo mass bins, with error bars corresponding to 1σ statistical errors. The solid lines correspond to weighted least-squares fits for each halo mass bin. Top left: unweighted sample, for galaxies with $\log(M_{\text{star}}/M_\odot) > 10.5$. Top right: unweighted sample, for galaxies with $\log(M_{\text{star}}/M_\odot) > 10.0$. Bottom left: V_{max} -weighted sample, for galaxies with $\log(M_{\text{star}}/M_\odot) > 9.0$. Bottom right: V_{max} -weighted sample, for galaxies with $\log(M_{\text{star}}/M_\odot) > 8.5$. Note that different mass scales are used in each panel. There are more halo mass bins in the bottom row due to the increased number of low-mass galaxies as a result of V_{max} weighting.

In Fig. 2.1 we plot mean stellar mass as a function of radial distance from the group centre for various halo mass bins. Fig 2.1(a) corresponds to our

high-mass cut, unweighted sample; Fig 2.1(b) corresponds to our low-mass cut, unweighted sample; Fig 2.1(c) corresponds to our high-mass cut, weighted sample; and Fig 2.1(d) corresponds to our low-mass cut, weighted sample.

For all halo mass bins, and regardless of the mass cut, the unweighted sample shows statistically significant mass segregation with a weighted linear least-squares fit. The V_{max} -weighted sample shows statistically significant mass segregation for the five lower halo mass bins, whereas the highest halo mass bin has a best-fitting slope consistent with zero – this trend hold for both mass cuts. For both the weighted and unweighted samples there is a clear trend of the slope with halo mass – more massive haloes show weaker mass segregation. This result will be discussed in Section ...

We find that our highest halo mass sample ($M_{\text{halo}} > 10^{14.5} M_{\odot}$) has a large number of low-mass galaxies when compared to the high-halo-mass samples, which leads to a smaller mean stellar mass in the V_{max} -weighted results shown in Figs 2.1(c) and (d). While this introduces a shift in normalization, it does not affect the mass segregation trend and therefore does not change the key result that mass segregation depends on halo mass.

2.3.2 Massive galaxy fraction

An alternative way to investigate galaxy populations within the group sample is to study the fraction of ‘massive’ galaxies at various group-centric radii. In Fig..., we plot the fraction of massive galaxies as a function of radial distance for two different definitions of what constitutes a massive galaxy. We calculate the massive fraction for each radial bin as

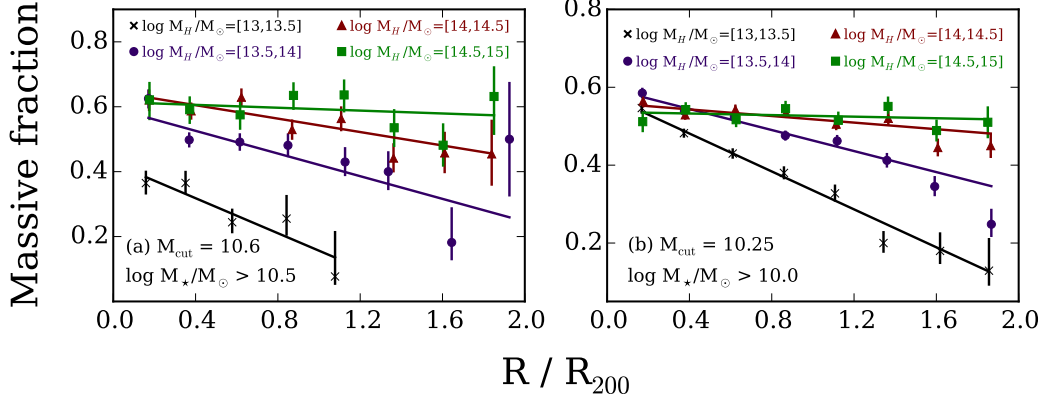


Figure 2.2 Fraction of massive galaxies with respect to normalized radial distance. Error bars are given by a 1σ binomial confidence interval, calculated using the beta distribution as outlined in Cameron (2011). The solid lines correspond to weighted least-squares fits for each halo mass bin. Left-hand panel: the fraction of galaxies with $\log(M_{\text{star}}/M_\odot) > 10.25$ as a function of radial distance, for the unweighted sample with $M_{\text{star}} > 10^{10}M_\odot$. Right-hand panel: the fraction of galaxies with $\log(M_{\text{star}}/M_\odot) > 10.5$ as a function of radial distance, for the unweighted sample with $M_{\text{star}} > 10^{10}M_\odot$.

$$f_m(M_{\text{cut}}) = \frac{\# \text{ galaxies with } M_{\text{star}} > M_{\text{cut}}}{\# \text{ galaxies with } M_{\text{star}} > 10^{10}M_\odot}, \quad (2.5)$$

where M_{cut} is a stellar mass cut-off above which we define a massive galaxy. We initially apply a high-mass galaxy cut, M_{cut} , at $10^{10.25}M_\odot$, corresponding to the median stellar mass of the unweighted sample (with the low-mass cut at $10^{10}M_\odot$). Comparing Figs 2.1(b) and 2.2(a) we see essentially identical trends. We observe the same trends of mass segregation whether we look at the average galaxy mass at a given radius, or consider the fraction of massive galaxies.

To confirm that this trend is robust regardless of the mass cut-off used to define a massive galaxy, we make the same plot but now use $M_{\text{cut}} = 10^{10.5}M_\odot$. Comparing Figs 2.2(a) and (b) we see that while the overall fractions of massive

galaxies decrease with increasing the stellar mass cut, the trend essentially stays the same. There is clear evidence for mass segregation and the strength of mass segregation depends on halo mass.

2.4 Discussion

2.4.1 Effect of including low-mass galaxies

The results in Fig. 2.1 show that mass segregation generally increases when lower mass galaxies are included. To quantify this effect we can compare the best-fitting slopes corresponding to the high-mass and the low-mass cut samples.

For a given halo mass, the low-mass cut sample displays larger slopes than the high-mass cut sample for two of the halo mass bins. The slopes corresponding to the other two halo mass bins are consistent with being equal. For the weighted samples we find similar results with the low-mass cut sample showing larger slopes for three of the halo mass bins, and the other three halo mass bins showing slopes consistent with being equal.

This suggests that the inclusion of low-mass galaxies has a measurable effect on the observation of mass-segregation. Studies which make mass cuts at moderate to high-stellar mass, are potentially missing a mass segregation contribution from low-mass galaxies. The observation of mild mass segregation is consistent with the low redshift sample of Ziparo et al. (2013); however, they see similar mass-radius relations regardless of the stellar mass cut applied.

2.4.2 Halo mass dependence

Figs 2.1 and 2.2 clearly indicate that the highest halo mass bins show the least mass segregation. This trend is consistent in all cases, regardless of stellar mass cut or whether the sample had V_{max} weights applied. Our observed dependence on halo mass is consistent with results finding no measurable mass segregation in galaxy clusters (Pracy et al., 2005; von der Linden et al., 2010; Vulcani et al., 2013)

It has been shown through N -body simulations that the dynamical friction time-scale scales with M_h/M_s (e.g. Taffoni et al., 2003; Conroy et al., 2007; Boylan-Kolchin et al., 2008), where M_s is the initial satellite mass and M_h is the mass of the host halo. For a given satellite mass, this implies a longer dynamical friction time-scale for larger haloes, which is consistent with our result. This can be interpreted as an increase in tidal stripping efficiency as M_h/M_s increases (Taffoni et al., 2003). Gan et al. (2010) have shown that for an infalling satellite the dynamical friction time-scale increases with a stronger tidal field. This is due to tidal stripping retarding the decay of satellite angular momentum, which increases the dynamical friction time-scale.

It should be noted that the merger time-scale scales with M_s/M_h Jiang et al. (2008), which implies a higher merger efficiency in low-mass haloes, for a given satellite mass. The build-up of massive objects through galaxy mergers could enhance mass segregation in low-mass haloes, in accordance with our results.

There has been evidence of cluster galaxies having their star formation quenched in lower mass groups ($\sim 10^{13}M_{\odot}$) prior to accretion into the cluster

environment (e.g. Zabludoff & Mulchaey, 1998; McGee et al., 2009; De Lucia et al., 2012; Hou et al., 2014). This pre-processing could potentially provide an explanation of our observed mass segregation trends with halo mass. If mass segregation is present in the group environment as a result of pre-processing, the recent accretion of multiple pre-processed groups to form a galaxy cluster could result in little to no observed mass segregation in the cluster as a whole. In other words, if the cluster environment consists of multiple subhaloes at various cluster-centric radii, while individual subhaloes may show mass segregation, the total effect of these subhaloes together may leave the cluster with a relatively uniform radial mass distribution.

Vulcani et al. (2014) apply semi-analytic models to the Millenium Simulation (Springel et al., 2005) to study galaxy mass functions in different environments. Vulcani et al. simulate galaxy mass functions for three halo masses, $\log(M_{\text{halo}}/M_{\odot}) = \{13.4, 14.1, 15.1\}$, as a function of cluster-centric radius. In the lowest mass halo they find the mass function depends slightly on cluster-centric radius, with the innermost regions showing flatter mass functions at low and intermediate masses. This trend persists, but is not as strong at intermediate halo mass. The highest halo mass bin shows virtually identical mass function shapes for all cluster-centric radii. This result is indicative of measurable mass segregation for the low- and intermediate-mass haloes, with the strength of mass segregation decreasing with increasing halo mass. These simulation trends show excellent agreement with our observed dependence of mass segregation on halo mass.

2.4.3 Reconciling previous results

In Section 2.1, we mention previous literature results which present evidence both for and against the presence of mass segregation in groups and clusters. We argue that the majority of these results can be reconciled with our two main findings.

- (i) Mass segregation is enhanced with the inclusion of low-mass galaxies in a sample.
- (ii) Mass segregation decreases with increasing halo mass, with high-mass haloes showing little to no mass segregation.

Of the studies mentioned in Section 2.1, those which observe no evidence for mass segregation either: make a mass completeness cut at intermediate to high stellar mass, or observe this lack of mass segregation only in high-mass haloes. Therefore, the lack of observed mass segregation can potentially be explained through the lack of low-mass galaxies in the study survey, or the study being limited to high-halo-mass environments.

2.5 Conclusion

In this Letter, we examine mass segregation trends in the Yang et al. (2007) SDSS DR7 groups for various stellar and halo mass cuts. We show that a small, but significant, amount of mass segregation is present in these groups. This mass segregation shows consistent trends, with lower stellar mass samples showing stronger mass segregation, and galaxies in large haloes showing little to no mass segregation.

The magnitude of mass segregation we measure, especially in high-mass haloes, is potentially indicative of dynamical friction not acting efficiently. We discuss previous literature to provide possible explanations for the observed trends, showing that our observed trends with halo mass agree with prior results. Further work with hydrodynamic simulations would be helpful to further constrain the important mechanisms responsible for our observed mass trends and the lack of mass segregation in high-mass haloes.

2.6 Acknowledgements

We thank the anonymous referee for their various helpful comments and suggestions. IDR and LCP thank the National Science and Engineering Research Council of Canada for funding. We thank X. Yang et al. for making their SDSS DR7 group catalogue public, L. Simard et al. for the publication of their SDSS DR7 morphology catalogue, and the NYU-VAGC team for the publication of their SDSS DR7 catalogue. This research would not have been possible without these public catalogues.

Funding for the SDSS has been provided by the Alfred P. Sloan Foundation, the Participating Institutions, the National Science Foundation, the US Department of Energy, the National Aeronautics and Space Administration, the Japanese Monbukagakusho, the Max Planck Society, and the Higher Education Funding Council for England. The SDSS website is <http://www.sdss.org/>.

Bibliography

- Abazajian, K. N., Adelman-McCarthy, J. K., Agüeros, M. A., Allam, S. S., Allende Prieto, C., An, D., Anderson, K. S. J., Anderson, S. F., Annis, J., Bahcall, N. A., & et al. 2009, *ApJS*, 182, 543
- Ball, N. M., Loveday, J., & Brunner, R. J. 2008, *MNRAS*, 383, 907
- Balogh, M. L., McGee, S. L., Mok, A., Wilman, D. J., Finoguenov, A., Bower, R. G., Mulchaey, J. S., Parker, L. C., & Tanaka, M. 2014, *MNRAS*, 443, 2679
- Balogh, M. L., Navarro, J. F., & Morris, S. L. 2000, *ApJ*, 540, 113
- Blanton, M. R., Eisenstein, D., Hogg, D. W., Schlegel, D. J., & Brinkmann, J. 2005a, *ApJ*, 629, 143
- Blanton, M. R. & Roweis, S. 2007, *AJ*, 133, 734
- Blanton, M. R., Schlegel, D. J., Strauss, M. A., Brinkmann, J., Finkbeiner, D., Fukugita, M., Gunn, J. E., Hogg, D. W., Ivezić, Ž., Knapp, G. R., Lupton, R. H., Munn, J. A., Schneider, D. P., Tegmark, M., & Zehavi, I. 2005b, *AJ*, 129, 2562
- Boylan-Kolchin, M., Ma, C.-P., & Quataert, E. 2008, *MNRAS*, 383, 93
- Brough, S., Forbes, D. A., Kilborn, V. A., & Couch, W. 2006, *MNRAS*, 370, 1223

- Cameron, E. 2011, PASA, 28, 128
- Carlberg, R. G., Yee, H. K. C., Ellingson, E., Morris, S. L., Abraham, R., Gravel, P., Pritchet, C. J., Smecker-Hane, T., Hartwick, F. D. A., Hesser, J. E., Hutchings, J. B., & Oke, J. B. 1997, ApJ, 485, L13
- Chabrier, G. 2003, PASP, 115, 763
- Chandrasekhar, S. 1943, ApJ, 97, 255
- Conroy, C., Ho, S., & White, M. 2007, MNRAS, 379, 1491
- De Lucia, G., Weinmann, S., Poggianti, B. M., Aragón-Salamanca, A., & Zaritsky, D. 2012, MNRAS, 423, 1277
- Eke, V. R., Baugh, C. M., Cole, S., Frenk, C. S., King, H. M., & Peacock, J. A. 2005, MNRAS, 362, 1233
- Gan, J.-L., Kang, X., Hou, J.-L., & Chang, R.-X. 2010, Research in Astronomy and Astrophysics, 10, 1242
- Geller, M. J. & Huchra, J. P. 1983, ApJS, 52, 61
- Hogg, D. W., Blanton, M. R., Brinchmann, J., Eisenstein, D. J., Schlegel, D. J., Gunn, J. E., McKay, T. A., Rix, H.-W., Bahcall, N. A., Brinkmann, J., & Meiksin, A. 2004, ApJ, 601, L29
- Hou, A., Parker, L. C., & Harris, W. E. 2014, MNRAS, 442, 406
- Jiang, C. Y., Jing, Y. P., Faltenbacher, A., Lin, W. P., & Li, C. 2008, ApJ, 675, 1095

McGee, S. L., Balogh, M. L., Bower, R. G., Font, A. S., & McCarthy, I. G. 2009, MNRAS, 400, 937

Oemler, Jr., A. 1974, ApJ, 194, 1

Poggianti, B. M., Desai, V., Finn, R., Bamford, S., De Lucia, G., Varela, J., Aragón-Salamanca, A., Halliday, C., Noll, S., Saglia, R., Zaritsky, D., Best, P., Clowe, D., Milvang-Jensen, B., Jablonka, P., Pelló, R., Rudnick, G., Simard, L., von der Linden, A., & White, S. 2008, ApJ, 684, 888

Pracy, M. B., Driver, S. P., De Propriis, R., Couch, W. J., & Nulsen, P. E. J. 2005, MNRAS, 364, 1147

Presotto, V., Iovino, A., Scodeggio, M., Cucciati, O., Knobel, C., Bolzonella, M., Oesch, P., Finoguenov, A., Tanaka, M., Kovač, K., Peng, Y., Zamorani, G., Bardelli, S., Pozzetti, L., Kampczyk, P., López-Sanjuan, C., Vergani, D., Zucca, E., Tasca, L. A. M., Carollo, C. M., Contini, T., Kneib, J.-P., Le Fèvre, O., Lilly, S., Mainieri, V., Renzini, A., Bongiorno, A., Caputi, K., de la Torre, S., de Ravel, L., Franzetti, P., Garilli, B., Lamareille, F., Le Borgne, J.-F., Le Brun, V., Maier, C., Mignoli, M., Pellò, R., Perez-Montero, E., Ricciardelli, E., Silverman, J. D., Tresse, L., Barnes, L., Bordoloi, R., Cappi, A., Cimatti, A., Coppa, G., Koekemoer, A. M., McCracken, H. J., Moresco, M., Nair, P., & Welikala, N. 2012, A&A, 539, A55

Simard, L., Mendel, J. T., Patton, D. R., Ellison, S. L., & McConnachie, A. W. 2011, ApJS, 196, 11

Springel, V., White, S. D. M., Jenkins, A., Frenk, C. S., Yoshida, N., Gao, L., Navarro, J., Thacker, R., Croton, D., Helly, J., Peacock, J. A., Cole,

- S., Thomas, P., Couchman, H., Evrard, A., Colberg, J., & Pearce, F. 2005, *Nature*, 435, 629
- Taffoni, G., Mayer, L., Colpi, M., & Governato, F. 2003, *MNRAS*, 341, 434
- Tal, T., Dekel, A., Oesch, P., Muzzin, A., Brammer, G. B., van Dokkum, P. G., Franx, M., Illingworth, G. D., Leja, J., Magee, D., Marchesini, D., Momcheva, I., Nelson, E. J., Patel, S. G., Quadri, R. F., Rix, H.-W., Skelton, R. E., Wake, D. A., & Whitaker, K. E. 2014, *ApJ*, 789, 164
- van den Bosch, F. C., Pasquali, A., Yang, X., Mo, H. J., Weinmann, S., McIntosh, D. H., & Aquino, D. 2008, *ArXiv e-prints*
- von der Linden, A., Wild, V., Kauffmann, G., White, S. D. M., & Weinmann, S. 2010, *MNRAS*, 404, 1231
- Vulcani, B., De Lucia, G., Poggianti, B. M., Bundy, K., More, S., & Calvi, R. 2014, *ApJ*, 788, 57
- Vulcani, B., Poggianti, B. M., Oemler, A., Dressler, A., Aragón-Salamanca, A., De Lucia, G., Moretti, A., Gladders, M., Abramson, L., & Halliday, C. 2013, *A&A*, 550, A58
- Wetzel, A. R., Tinker, J. L., & Conroy, C. 2012, *MNRAS*, 424, 232
- Wetzel, A. R., Tinker, J. L., Conroy, C., & van den Bosch, F. C. 2013, *MNRAS*, 432, 336
- Yang, X., Mo, H. J., van den Bosch, F. C., & Jing, Y. P. 2005, *MNRAS*, 356, 1293

Yang, X., Mo, H. J., van den Bosch, F. C., Pasquali, A., Li, C., & Barden, M.
2007, *ApJ*, 671, 153

Zabludoff, A. I. & Mulchaey, J. S. 1998, *ApJ*, 496, 39

Ziparo, F., Popesso, P., Biviano, A., Finoguenov, A., Wuyts, S., Wilman, D.,
Salvato, M., Tanaka, M., Ilbert, O., Nandra, K., Lutz, D., Elbaz, D., Dick-
inson, M., Altieri, B., Aussel, H., Berta, S., Cimatti, A., Fadda, D., Genzel,
R., Le Flo'ch, E., Magnelli, B., Nordon, R., Poglitsch, A., Pozzi, F., Portal,
M. S., Tacconi, L., Bauer, F. E., Brandt, W. N., Cappelluti, N., Cooper,
M. C., & Mulchaey, J. S. 2013, *MNRAS*, 434, 3089

Chapter 3

Comparing galaxy morphology and star formation properties in X-ray bright and faint groups and cluster

3.1 Introduction

Numerous studies have shown a strong environmental dependence on the star-forming and morphological properties of galaxies (e.g. Butcher & Oemler, 1978; Dressler, 1980; Postman & Geller, 1984; Dressler et al., 1999; Blanton et al., 2005a; Wetzel et al., 2012). Low-density regimes tend to be dominated by star-forming, late-type galaxies whereas high-density areas, such as galaxy clusters, tend to be primarily populated by quiescent, early-type galaxies. Within individual clusters, galaxy morphologies tend to distribute as a function of local density (or equivalently cluster-centric radius), with high fractions of late-type galaxies being found at large radii and the regions near the cluster core being dominated by early-types (e.g. Dressler, 1980; Postman & Geller, 1984; Postman et al., 2005). This effect has become known as the morphology-

density relation. While galaxies tends to distribute based on their star-forming and morphological properties, the mechanism(s) responsible for the quenching of star formation and morphological transformations in galaxies are not well constrained – although many have been proposed. Both mergers and impulsive galaxy-galaxy interactions (‘harassment’) (e.g. Moore et al., 1996) can induce starburst events in galaxies leading to rapid consumption of gas reserves and star formation quenching. Within the virial radius of a group or cluster the stripping of gas from galaxies becomes efficient. Both the stripping of hot halo gas (‘strangulation’) (e.g. Kawata & Mulchaey, 2008) and cold gas stripping due to a dense intracluster medium (‘ram-pressure’) (e.g. Gunn & Gott, 1972) can quench star formation. As well, tidal interactions can affect gas reservoirs by transporting gas from the galactic halo outwards which subsequently allows it to more easily be stripped from the galaxy (Chung et al., 2007).

On top of these environmental quenching mechanisms, previous authors have found that secular processes, which depend on galaxy mass, appear to play a significant role in star formation quenching (Balogh et al., 2004; Muzzin et al., 2012). The emergent picture for star formation quenching appears to be some combination of environmental quenching mechanisms and internal, secular processes. In particular, (Peng et al., 2010) suggests that in the low-redshift Universe, environmental quenching is dominant for galaxies with $M_{\star} \lesssim 10^{10.5} M_{\odot}$, whereas for galaxies with $M_{\star} \gtrsim 10^{10.5} M_{\odot}$ mass quenching plays the more important role.

While environmental and mass quenching within individual haloes are seemingly strong effects, it is important to realize that groups and clusters are

not isolated structures. In particular, galaxies can be pre-quenched in group haloes prior to infall into a larger cluster. This ‘pre-processing’ suggests that many galaxies may already be quenched upon cluster infall. Simulations have shown that between ~ 25 and 45 per cent of infalling cluster galaxies may have been pre-processed (McGee et al., 2009; De Lucia et al., 2012). Observationally, (Hou et al., 2014) find that ~ 25 per cent of the infall population reside in subhaloes for massive clusters ($M_H \gtrsim 10^{14.5} M_\odot$). This pre-quenching of galaxies in groups could potentially be driven by galaxy interactions and mergers which are favoured in the group regime as a result of lower relative velocities between member galaxies (Barnes, 1985; Brough et al., 2006).

An important method for study the quenching mechanisms in groups and clusters is to study the dependence of the star formation and morphological properties of galaxies on the conditions of their host halo (e.g. halo mass, X-ray luminosity, etc.). In particular, if quenching mechanisms depend on the density of the intra-group/cluster medium (IGM/ICM) – for example, ram-pressure stripping of cold gas – then one would expect to see galaxy populations which are preferentially passive in haloes with high X-ray luminosities. Such correlations have been looked for in previous studies, primarily within cluster environments.

In particular, Ellingson et al. (2001) find no positive correlation between the fraction of old galaxies and X-ray gas density. Balogh et al. (2002a) conclude that the level of star formation found in their ‘low- L_X ’ sample is consistent with the levels seen in their CNOC1 sample consisting of higher mass clusters. Fairley et al. (2002) and Wake et al. (2005) both study the fractions of blue

galaxies at intermediate redshifts and find no discernible trend between blue fraction and X-ray luminosity. Using multivariate regression Popesso et al. (2007) find that cluster star formation depends on cluster richness but find no additional dependence on X-ray luminosity. In addition, they find no significant correlation between star-forming fraction and any global cluster property (M_{200} , σ_v , N_{gal} , and L_X). Lopes et al. (2014) find no dependence of blue fraction on X-ray luminosity and the only slight dependence they find between disc fraction and X-ray luminosity is within the central and most dense regions.

Conversely, Balogh et al. (2002b) find that galaxies in their ‘low- L_X ’ sample have preferentially high disc fractions compared to galaxies in their ‘high- L_X ’ sample. Postman et al. (2005) find that the bulge-dominated fraction for galaxies in high X-ray luminosity clusters is higher than for those in low X-ray luminosity clusters. In contrast with their star formation results, Popesso et al. (2007) do find a significant anticorrelation between blue fraction and X-ray luminosity. Finally, Urquhart et al. (2010) find an anticorrelation between blue fraction and X-ray temperature for galaxies in intermediate redshift clusters.

In this paper we revisit the dependence of galaxy star formation and morphological properties on the X-ray luminosity of the host halo. Specifically, as a result of the large SDSS X-ray sample presented in Wang et al. (2014), we are able to control for stellar mass, halo mass, and radial dependences through fine-binning of the data set. This allows us to more directly investigate the effect of X-ray luminosity on galaxies in different environments.

The results of this study are presented as follows. In Section 3.2 we briefly describe the SDSS group catalogues utilized in this work, as well as the star

formation and morphology catalogues which we match to the group data set. In Section 3.3 we present the primary results of this paper, specifically, the differences between star-forming and morphological trends in environments with different X-ray luminosities. In Section 3.4 we provide a discussion of the results presented in this paper. Finally, in Section 3.5 we provide a summary of the key results and make concluding statements.

In this paper we assume a Λ cold dark matter cosmology with $\Omega_M = 0.3$, $\Omega_\Lambda = 0.7$, and $H_0 = 70 \text{ km s}^{-1} \text{ Mpc}^{-1}$.

3.2 Data

3.2.1 Yang group catalogue

This work relies heavily on the group catalogue of Yang et al. (2007). The Yang group catalogue is constructed by applying the iterative halo-based group finder of Yang et al. (2005, 2007) to the New York University Value-Added Galaxy Catalogue (NYU-VAGC; Blanton et al. 2005b), which is based on the Sloan Digital Sky Survey Data Release 7 (SDSS-DR7; Abazajian et al. 2009). The Yang group catalogue has a wide range of halo masses, spanning from $\sim 10^{12} M_\odot$ to $\sim 10^{15} M_\odot$. The catalogue contains both objects which would be classified as groups ($10^{12} \lesssim M_H \lesssim 10^{14}$) and as clusters ($M_H \gtrsim 10^{14} M_\odot$), however for brevity we will refer to all systems as groups regardless of mass.

Groups are initially populated using the traditional friends-of-friends (FOF) algorithm (e.g. Huchra & Geller, 1982), as well as assigning galaxies not yet

linked to FOF groups as the centres of potential groups. Next, the characteristic luminosity, $L_{19.5}$, defined as the combined luminosity of all group members with ${}^{0.1}M_r - 5 \log h \leq -19.5$, is calculated for each group. Using the value of $L_{19.5}$ along with an assumption for the group mass-to-light ratio, $M_H/L_{19.5}$, a tentative halo mass is assigned on a group-by-group basis. The tentative halo mass is used to calculate a virial radius and velocity dispersion for each group, which are then used to add or remove galaxies from the system. Galaxies are assigned to groups under the assumption that the distribution of galaxies in phase space follows that of dark matter particles – the distribution of which is assumed to follow a spherical NFW profile (Navarro et al., 1997). This process is iterated until the group memberships no longer change.

Final halo masses given in the Yang group catalogue are determined using the ranking of the characteristic stellar mass, $M_{\star, \text{grp}}$, and assuming a relationship between M_H and $M_{\star, \text{grp}}$ (Yang et al., 2007). $M_{\star, \text{grp}}$ is defined by Yang et al. as

$$M_{\star, \text{grp}} = \frac{1}{g(L_{19.5}, L_{\text{lim}})} \sum_i \frac{M_{\star, i}}{C_i}, \quad (3.1)$$

where $M_{\star, i}$ is the stellar mass of the i th member galaxy, C_i is the completeness of the survey at the position of that galaxy, and $g(L_{19.5}, L_{\text{lim}})$ is a correction factor which accounts for galaxies missed due to the magnitude limit of the survey. The statistical error in M_H is on the order of 0.3 dex and mostly independent of halo mass (Yang et al., 2007).

3.2.2 SDSS X-ray catalogue

To study the X-ray properties of the group sample, we utilize the SDSS X-ray catalogue of Wang et al. (2014), which combines ROSAT All Sky Survey (RASS) X-ray images in conjunction with optical groups identified from SDSS-DR7 (Yang et al., 2007) to estimate X-ray luminosities around $\sim 65\,000$ spectroscopic groups.

To identify X-ray luminosities for individual groups, the algorithm of Shen et al. (2008) is employed. Beginning from an optical group, the most massive galaxies (MMGs) of that group are identified – up to four MMGs are kept. The RASS field in which the MMGs reside are then identified, and an X-ray source catalogue is generated in the 0.5–2.0 keV band (Wang et al., 2014). The maximum X-ray emission density point is used to identify the X-ray centre of the group, and any X-ray sources not associated with the group (e.g. point source quasars or stellar object cross-matched from RASS and SDSS-DR7), within one virial radius, are masked out. Values for the X-ray background, centred on the X-ray centre, are determined and subtracted off and the X-ray luminosity, L_X , is calculated by integrating the source count profile within the X-ray radius.

Determining X-ray luminosities in this manner is susceptible to ‘source confusion’. Due to projection it is possible for more than one group to contribute to the X-ray emission within the X-ray radius, leading to an overestimation of the X-ray luminosity for a given group. To account for this effect Wang et al. (2014) calculate the ‘expected’ average X-ray flux, $F_{X,i}$, for each group using the average $L_X - M_H$ relation taken from Mantz et al. (2010). They then cal-

culate the sum of the expected fluxes from each group for multigroup systems and determine the contribution fraction, $f_{\text{mult},i}$, for each group defined as

$$f_{\text{mult},i} = F_{X,i} / \sum_i F_{X,i}. \quad (3.2)$$

The contribution factor will approximate the fraction of the observed X-ray luminosity intrinsic to the individual group in question, therefore applying this fraction to each group will act to debias the measured X-ray luminosity from source confusion contamination.

Within the Wang catalogue 817 groups have $S/N > 3$, compared to the total of 34 522 groups with positive detections (positive count rates after background subtraction) and $S/N > 0$. We run our analysis for groups with $S/N > 3$ as well as groups with $S/N > 0$ and find that our choice of signal-to-noise cut does not change the trends that we observe, therefore we focus on the total sample ($S/N > 0$) to ensure a sample size which is large enough to finely bin the data in various properties simultaneously.

3.2.3 Final data set

To obtain the final data set, we match the Wang SDSS X-ray catalogue to the Yang SDSS group catalogue, giving us both optical and X-ray group properties for the sample. To obtain individual galaxy properties we further match the data set to various public SDSS catalogues as follows.

We utilize stellar masses given in the NYU-VAGC, which are computed following the methodology of Blanton & Roweis (2007).

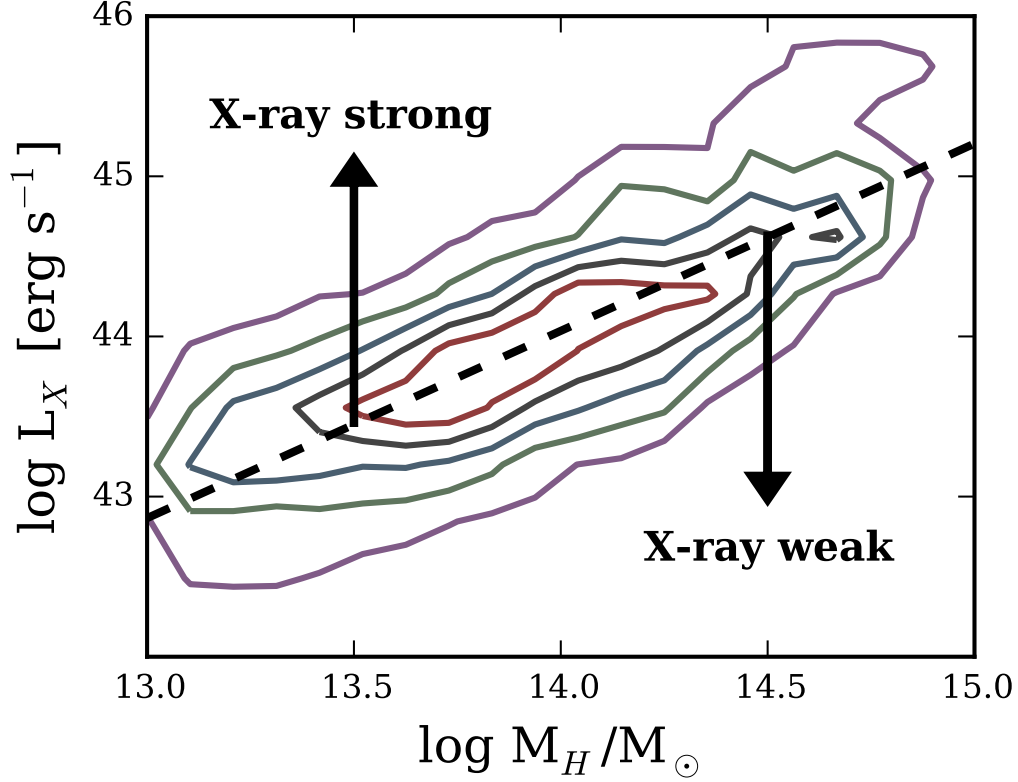


Figure 3.1 Density contours for log X-ray luminosity versus log halo mass. Dashed line corresponds to the linear least-squares best-fitting relationship.

To obtain star formation rates (SFRs) and specific star formation rates ($\text{SSFR} = \text{SFR}/M_\star$) we match the catalogue of Brinchmann et al. (2004) to the sample. SFRs given by Brinchmann et al. are determined using emission line fluxes whenever possible; however, in the case of no clear emission lines or contamination from active galactic nuclei (AGNs), SFRs are determined using the strength of the 4000 Å break (D_n4000) (Brinchmann et al., 2004).

We obtain galaxy morphologies from the catalogue of Simard et al. (2011). Simard et al. perform two-dimensional bulge + disc decompositions for over one million galaxies from the Legacy area of the SDSS-DR7, using three dif-

ferent fitting models: a pure Sérsic model, a bulge + disc model with a de Vaucouleurs ($n_b = 4$) bulge, and a bulge + disc model with a free n_b . To distinguish between discy and elliptical galaxies we utilize the galaxy Sérsic index, n_g , from the pure Sérsic decomposition. We also use the V_{\max} weights given by Simard et al. to correct for the incompleteness of our sample.

We calculate group-centric distances for each galaxy using the redshift of the group and the angular separation between the galaxy and the luminosity-weighted centre of its host group. We normalize all of the galaxy radii by the virial radius of the host group, R_{180} , which we calculate as in Yang et al. (2007)

$$R_{180} = 1.26 h^{-1} \text{ Mpc} \left(\frac{M_H}{10^{14} h^{-1} \text{ M}_\odot} \right)^{1/3} (1 + z_g)^{-1}, \quad (3.3)$$

where z_g is the redshift of the group centre.

The final data set includes groups with halo masses ranging between $10^{13} - 10^{15} \text{ M}_\odot$, and galaxies with stellar masses ranging from $10^9 - 10^{11.3} \text{ M}_\odot$. Group X-ray luminosities in the data set are between $10^{39.6} - 10^{46.4} \text{ erg s}^{-1}$, with a median value of $10^{43.9} \text{ erg s}^{-1}$, and are strongly correlated with halo mass (see Fig. 3.1). We do not make an explicit radial cut, however over 99 per cent of member galaxies fall within 1.5 virial radii. Our final sample contains 3 902 low-redshift ($z < 0.1$) groups hosting 41 173 galaxies. The catalogue of Wang et al. (2014) contains $\sim 35\,000$ groups. The fact that the final sample in this work is significantly smaller than the original catalogue is twofold. First, we restrict our sample to redshifts smaller than 0.1 which reduces the number of groups from $\sim 35\,000$ at $z < 0.2$ to $\sim 18\,000$ at $z < 0.1$. The second important cut is that we require $10^{13} < M_H < 10^{15} \text{ M}_\odot$ and a number of groups in the

Wang catalogue have halo masses, $M_H < 10^{13} M_\odot$ (where halo masses have been obtained from the catalogue of Yang et al. 2007). This cut reduces the remaining number of groups from $\sim 18\,000$ to $\sim 3\,900$. It should be noted that the majority of the $M_H < 10^{13} M_\odot$ groups removed from the data set are groups with very low membership.

To determine the effect of X-ray luminosity on star formation and morphology we consider two X-ray luminosity samples for the majority of our analysis, which we refer to as the X-ray weak (XRW) and X-ray strong (XRS) samples. Similar to Wang et al. (2014), we define the XRS sample to consist of all galaxies found below the $\log M_H - \log L_X$ trend line. This leads to an approximately equal number of galaxies within the XRW and XRS samples. We also performed our analysis with a cut between the two X-ray samples at the median X-ray luminosity of the data set, as well as defining the two samples using the first and the fourth quartiles, however these alternative definitions of the two X-ray samples do not change the trends that we observe.

Smoothed distributions for halo mass and X-ray luminosity are shown in Fig. 3.2 for both X-ray luminosity samples. Density distributions are calculated using the `density {stats}` function in the statistical computing language R (R Core Team, 2013)¹ using a Gaussian kernel.

We study the dependence of star formation rates and morphology on stellar mass by binning the data by stellar mass and calculating the disc and star-forming fractions for each bin. Binning by stellar mass is important to account for the systematic dependence of star formation and morphology on stellar

¹ <http://www.R-project.org/>

mass (e.g. Brinchmann et al., 2004; Whitaker et al., 2012). Additionally, as the relative balance between environmental and mass quenching is not well understood, it is important to investigate the effects of environment at a given stellar mass.

We define the star-forming fraction, f_{SF} , as the fraction of galaxies in each bin with $\log \text{SSFR} > -11$. Wetzel et al. (2012) show that at low redshift the division between the red sequence and the blue cloud is found at $\log \text{SSFR} \simeq -11$ across a wide range of halo masses. For each stellar mass bin the star-forming fraction is given by

$$f_{SF} = \frac{V_{\text{max}} \text{ weighted no. of galaxies with } \log \text{SSFR} > -11}{V_{\text{max}} \text{ weighted total no. of galaxies}} \quad (3.4)$$

Similarly we define the disc fraction, f_D , as the fraction of galaxies in each bin with Sérsic index, $n < 1.5$. For each stellar mass bin this is given by

$$f_{SF} = \frac{V_{\text{max}} \text{ weighted no. of galaxies with } n < 1.5}{V_{\text{max}} \text{ weighted total no. of galaxies}} \quad (3.5)$$

We also ran our analysis using a dividing cut at Sérsic indices of $n = 1.0$ and $n = 2.0$ to define a disc galaxy, however using these alternative definitions for a disc galaxy does not alter the trends that we observe.

3.3 Results

3.3.1 Star-forming and morphology trends in strong and weak L_X samples

To investigate the effect of X-ray luminosity on galaxy properties, in Fig. 3.3 we show star-forming and disc fractions, as a function of stellar mass, for subsamples corresponding to the four X-ray luminosity quartiles of the data set. Examination of Figs 3.3(a) and (b) show that star-forming and disc fractions follow a consistent marching order with respect to X-ray luminosity. The disc and star-forming fractions decrease as X-ray luminosity increases.

We note that the results in Fig. 3.3 consider all halo masses in the sample, however it has been found that galaxy morphology and star formation depend on local density and halo mass (Dressler, 1980; Balogh et al., 2004; Wetzel et al., 2012; Lackner & Gunn, 2013) (however also see: De Lucia et al. 2012; Hoyle et al. 2012; Hou et al. 2013). As shown in Fig. 3.1 the data show a strong correlation between X-ray luminosity and halo mass, therefore we must determine if differences shown in Fig. 3.3 are simply a result of galaxies in higher L_X environments being housed in preferentially high-mass haloes.

To control for any potential halo mass effect, we further bin the data into narrow halo mass bins and re-examine the dependence of galaxy properties on X-ray luminosity, considering now the XRW and XRS samples from Fig. 3.1. Fig. 3.4 shows star-forming (solid) and disc (dashed) fractions as a function of stellar mass for four different halo mass bins – ranging from 10^{13} to $10^{15} M_\odot$ with bin widths of 0.5 dex. Data are binned according to stellar mass and

markers are plotted at the median bin values. For each halo mass bin we show star-forming and disc fractions from the X-ray strong and X-ray weak samples.

For both star-forming and disc fractions we continue to see a residual trend with X-ray luminosity, even after controlling for any halo mass dependence: star-forming and disc fractions are systematically higher in the XRW sample. We see the strongest trends in the intermediate and high-mass haloes. The difference between the strong (red) and weak (blue) X-ray luminosity samples is clearest at low stellar mass, and in all haloes the two samples converge at moderate to high stellar mass.

3.3.2 Radial dependence of star-forming and morphology trends

Within host groups X-ray emission is concentrated at relatively small group-centric radii, with X-ray emission generally extending out to half a virial radius (Wang et al., 2014). If the trends we are observing are a result of increased gas density, we would expect to see enhanced trends (i.e. a larger difference between the XRS and XRW samples) at small group-centric radii and suppressed trends at large radii. To test this we further divide the data into subsets corresponding to those galaxies that lie within the X-ray emission radius (using the X-ray radius, R_{Xray} , given in Wang et al. 2014) and those galaxies that lie outside of the X-ray radius. We again plot star-forming/disc fraction versus stellar mass, in narrow halo mass bins, for the large and small radius subsamples. The results of this analysis are shown in Figs 3.5 and 3.6, where the two figures correspond to disc fraction and star-forming fraction trends for the large and small radius subsamples, respectively.

Examination of Figs 3.5 and 3.6 shows that for both galaxies found within their host halo’s X-ray radius and those found outside, we still see an increase in star-forming and disc fractions in the XRW sample – as before this effect is strongest in the intermediate-to high-mass haloes and at low stellar mass. Also the disc and star-forming fractions tend to be higher at large radii, which is consistent with the morphology-density relation.

To further investigate if the increase in star-forming and disc fractions in the XRW sample compared to the XRS sample – which we will refer to as the ‘SF excess’ and the ‘disc excess’ – depends on whether you consider galaxies within or outside of the X-ray radius, we show SF and disc excess versus stellar mass in Fig. 3.7. We quantitatively define SF and disc excess as

$$\text{SF excess} = f_{SF}(\text{XRW}) - f_{SF}(\text{XRS}) \quad (3.6)$$

$$\text{Disc excess} = f_D(\text{XRW}) - f_D(\text{XRS}) \quad (3.7)$$

where $f_{SF}(\text{XRW})$ and $f_{SF}(\text{XRS})$ are the star-forming fractions in the XRW and XRS samples respectively, and analogously for $f_D(\text{XRW})$ and $f_D(\text{XRS})$.

We find no radial dependence for SF and disc excess as the two radial subsamples in Fig. 3.7 show overlap for all halo and stellar masses. With the exception in Fig. 3.7(c) where the SF excess, for low-mass galaxies, is stronger for galaxies within the X-ray radius.

3.4 Discussion

3.5 Summary & Conclusions

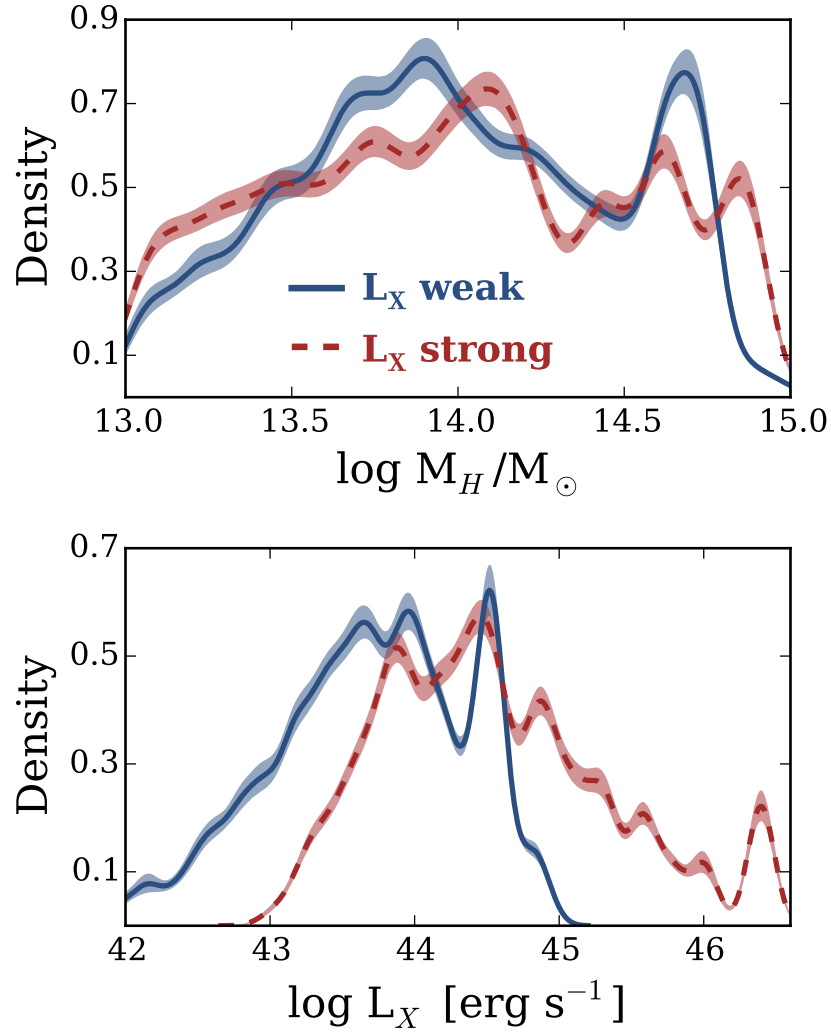


Figure 3.2 Smoothed distributions for halo mass and X-ray luminosity within the sample. Distributions are shown for both the X-ray strong (red, dashed) and the X-ray weak (blue, solid) samples. Shaded regions correspond to 2σ confidence intervals obtained from random bootstrap resampling.

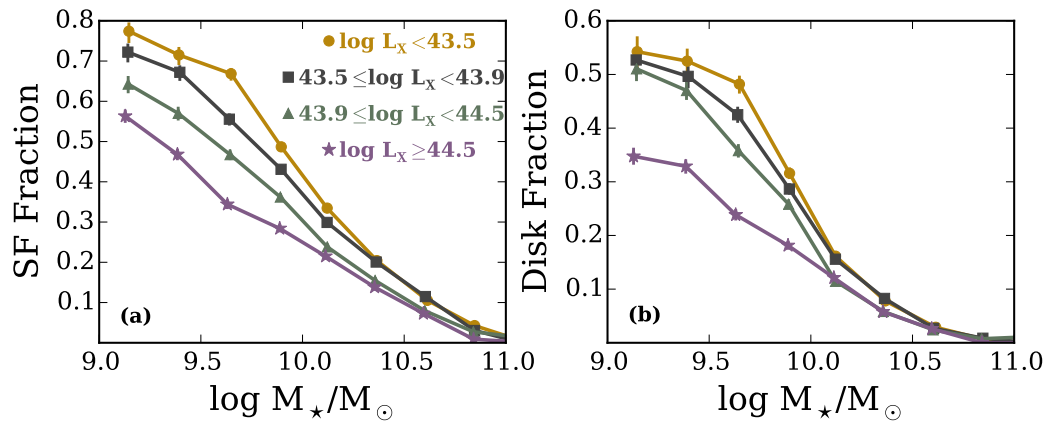


Figure 3.3 Left: star-forming fraction versus stellar mass for the four X-ray luminosity quartiles of the data sample. Right: disk fraction versus stellar mass for the four X-ray luminosity quartiles of the sample. Error bars correspond to 1σ Bayesian binomial confidence intervals given in Cameron (2011)

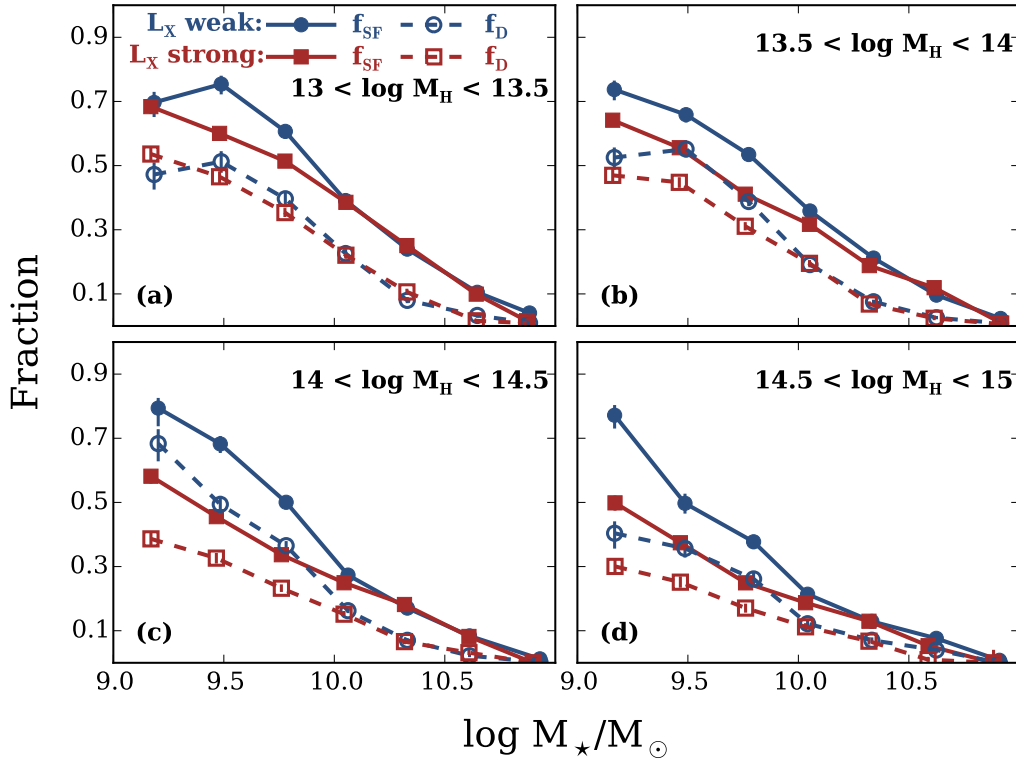


Figure 3.4 Star-forming (solid lines) and disc (dashed lines) fractions versus stellar mass, for different halo mass bins and the XRW (blue) and XRS (red) samples. Error bars correspond to 1σ Bayesian binomial confidence intervals given in Cameron (2011)

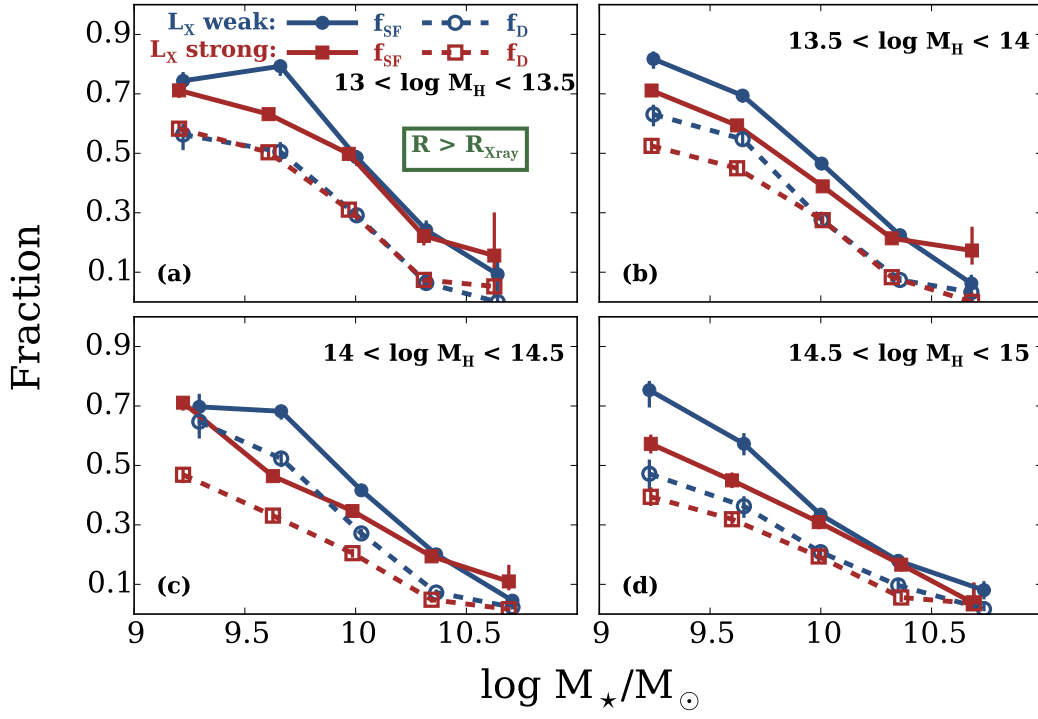


Figure 3.5 Star-forming (solid lines) and disc (dashed lines) fractions versus stellar mass, for galaxies outside of their host X-ray radius and for different halo mass bins and the two L_X samples. Error bars correspond to 1σ Bayesian binomial confidence intervals given in Cameron (2011)

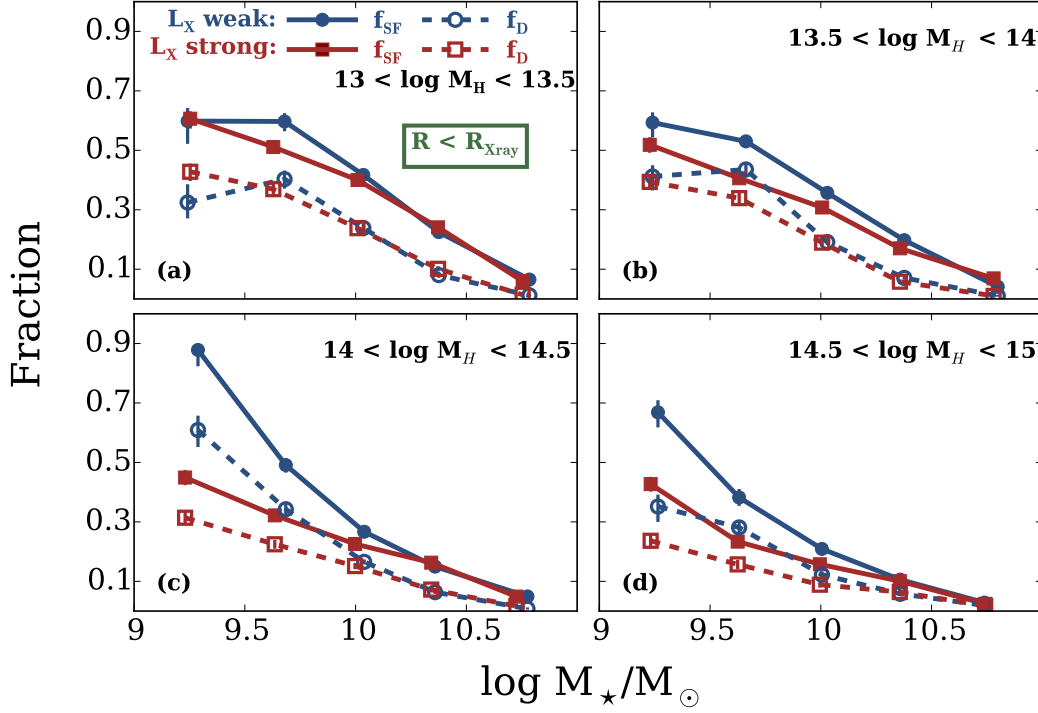


Figure 3.6 Same as Fig. 3.5 for galaxies inside of their host X-ray radius.

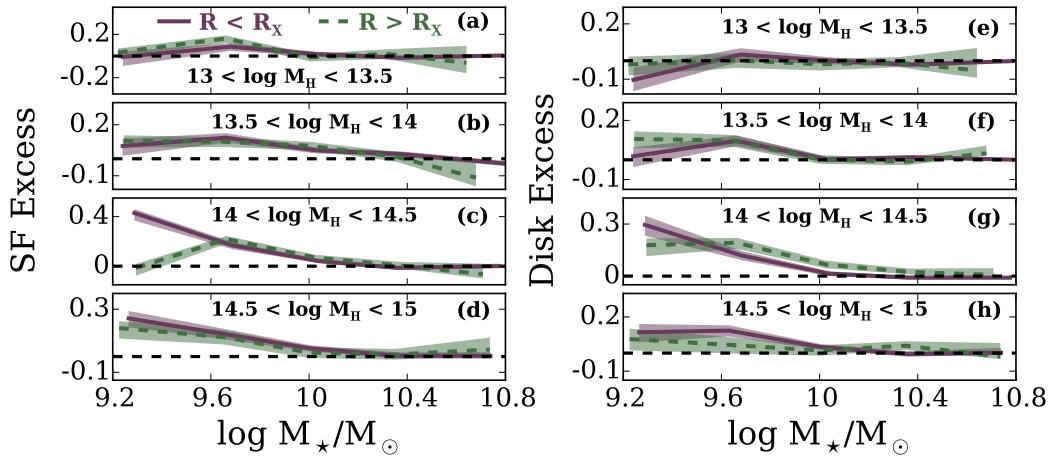


Figure 3.7 SF and disk excess versus stellar mass for both galaxies within (purple, solid) and outside (green, dashed) of the X-ray radius. Panels a-d show SF excess for four halo mass bins and panels e-h show disk excess for four halo mass bins. Shaded regions represent 1σ confidence intervals.

Bibliography

- Abazajian, K. N., Adelman-McCarthy, J. K., Agüeros, M. A., Allam, S. S., Allende Prieto, C., An, D., Anderson, K. S. J., Anderson, S. F., Annis, J., Bahcall, N. A., & et al. 2009, *ApJS*, 182, 543
- Balogh, M., Bower, R. G., Smail, I., Ziegler, B. L., Davies, R. L., Gaztelu, A., & Fritz, A. 2002a, *MNRAS*, 337, 256
- Balogh, M. L., Baldry, I. K., Nichol, R., Miller, C., Bower, R., & Glazebrook, K. 2004, *ApJ*, 615, L101
- Balogh, M. L., Smail, I., Bower, R. G., Ziegler, B. L., Smith, G. P., Davies, R. L., Gaztelu, A., Kneib, J.-P., & Ebeling, H. 2002b, *ApJ*, 566, 123
- Barnes, J. 1985, *MNRAS*, 215, 517
- Blanton, M. R., Eisenstein, D., Hogg, D. W., Schlegel, D. J., & Brinkmann, J. 2005a, *ApJ*, 629, 143
- Blanton, M. R. & Roweis, S. 2007, *AJ*, 133, 734
- Blanton, M. R., Schlegel, D. J., Strauss, M. A., Brinkmann, J., Finkbeiner, D., Fukugita, M., Gunn, J. E., Hogg, D. W., Ivezić, Ž., Knapp, G. R., Lupton, R. H., Munn, J. A., Schneider, D. P., Tegmark, M., & Zehavi, I. 2005b, *AJ*, 129, 2562

- Brinchmann, J., Charlot, S., White, S. D. M., Tremonti, C., Kauffmann, G., Heckman, T., & Brinkmann, J. 2004, MNRAS, 351, 1151
- Brough, S., Forbes, D. A., Kilborn, V. A., & Couch, W. 2006, MNRAS, 370, 1223
- Butcher, H. & Oemler, Jr., A. 1978, ApJ, 219, 18
- Cameron, E. 2011, PASA, 28, 128
- Chung, A., van Gorkom, J. H., Kenney, J. D. P., & Vollmer, B. 2007, ApJ, 659, L115
- De Lucia, G., Weinmann, S., Poggianti, B. M., Aragón-Salamanca, A., & Zaritsky, D. 2012, MNRAS, 423, 1277
- Dressler, A. 1980, ApJ, 236, 351
- Dressler, A., Smail, I., Poggianti, B. M., Butcher, H., Couch, W. J., Ellis, R. S., & Oemler, Jr., A. 1999, ApJS, 122, 51
- Ellingson, E., Lin, H., Yee, H. K. C., & Carlberg, R. G. 2001, ApJ, 547, 609
- Fairley, B. W., Jones, L. R., Wake, D. A., Collins, C. A., Burke, D. J., Nichol, R. C., & Romer, A. K. 2002, MNRAS, 330, 755
- Gunn, J. E. & Gott, III, J. R. 1972, ApJ, 176, 1
- Hou, A., Parker, L. C., Balogh, M. L., McGee, S. L., Wilman, D. J., Connelly, J. L., Harris, W. E., Mok, A., Mulchaey, J. S., Bower, R. G., & Finoguenov, A. 2013, MNRAS, 435, 1715

- Hou, A., Parker, L. C., & Harris, W. E. 2014, MNRAS, 442, 406
- Hoyle, B., Masters, K. L., Nichol, R. C., Jimenez, R., & Bamford, S. P. 2012, MNRAS, 423, 3478
- Huchra, J. P. & Geller, M. J. 1982, ApJ, 257, 423
- Kawata, D. & Mulchaey, J. S. 2008, ApJ, 672, L103
- Lackner, C. N. & Gunn, J. E. 2013, MNRAS, 428, 2141
- Lopes, P. A. A., Ribeiro, A. L. B., & Rembold, S. B. 2014, MNRAS, 437, 2430
- Mantz, A., Allen, S. W., Ebeling, H., Rapetti, D., & Drlica-Wagner, A. 2010, MNRAS, 406, 1773
- McGee, S. L., Balogh, M. L., Bower, R. G., Font, A. S., & McCarthy, I. G. 2009, MNRAS, 400, 937
- Moore, B., Katz, N., Lake, G., Dressler, A., & Oemler, A. 1996, Nature, 379, 613
- Muzzin, A., Wilson, G., Yee, H. K. C., Gilbank, D., Hoekstra, H., Demarco, R., Balogh, M., van Dokkum, P., Franx, M., Ellingson, E., Hicks, A., Nantais, J., Noble, A., Lacy, M., Lidman, C., Rettura, A., Surace, J., & Webb, T. 2012, ApJ, 746, 188
- Navarro, J. F., Frenk, C. S., & White, S. D. M. 1997, ApJ, 490, 493
- Peng, Y.-j., Lilly, S. J., Kovač, K., Bolzonella, M., Pozzetti, L., Renzini, A., Zamorani, G., Ilbert, O., Knobel, C., Iovino, A., Maier, C., Cucciati,

- O., Tasca, L., Carollo, C. M., Silverman, J., Kampczyk, P., de Ravel, L., Sanders, D., Scoville, N., Contini, T., Mainieri, V., Scodeggio, M., Kneib, J.-P., Le Fèvre, O., Bardelli, S., Bongiorno, A., Caputi, K., Coppa, G., de la Torre, S., Franzetti, P., Garilli, B., Lamareille, F., Le Borgne, J.-F., Le Brun, V., Mignoli, M., Perez Montero, E., Pello, R., Ricciardelli, E., Tanaka, M., Tresse, L., Vergani, D., Welikala, N., Zucca, E., Oesch, P., Abbas, U., Barnes, L., Bordoloi, R., Bottini, D., Cappi, A., Cassata, P., Cimatti, A., Fumana, M., Hasinger, G., Koekemoer, A., Leauthaud, A., Maccagni, D., Marinoni, C., McCracken, H., Memeo, P., Meneux, B., Nair, P., Porciani, C., Presotto, V., & Scaramella, R. 2010, *ApJ*, 721, 193
- Popesso, P., Biviano, A., Romaniello, M., & Böhringer, H. 2007, *A&A*, 461, 411
- Postman, M., Franx, M., Cross, N. J. G., Holden, B., Ford, H. C., Illingworth, G. D., Goto, T., Demarco, R., Rosati, P., Blakeslee, J. P., Tran, K.-V., Benítez, N., Clampin, M., Hartig, G. F., Homeier, N., Ardila, D. R., Bartko, F., Bouwens, R. J., Bradley, L. D., Broadhurst, T. J., Brown, R. A., Burrows, C. J., Cheng, E. S., Feldman, P. D., Golimowski, D. A., Gronwall, C., Infante, L., Kimble, R. A., Krist, J. E., Lesser, M. P., Martel, A. R., Mei, S., Menanteau, F., Meurer, G. R., Miley, G. K., Motta, V., Sirianni, M., Sparks, W. B., Tran, H. D., Tsvetanov, Z. I., White, R. L., & Zheng, W. 2005, *ApJ*, 623, 721
- Postman, M. & Geller, M. J. 1984, *ApJ*, 281, 95

- R Core Team. 2013, R: A Language and Environment for Statistical Computing, R Foundation for Statistical Computing, Vienna, Austria
- Shen, S., Kauffmann, G., von der Linden, A., White, S. D. M., & Best, P. N. 2008, MNRAS, 389, 1074
- Simard, L., Mendel, J. T., Patton, D. R., Ellison, S. L., & McConnachie, A. W. 2011, ApJS, 196, 11
- Urquhart, S. A., Willis, J. P., Hoekstra, H., & Pierre, M. 2010, MNRAS, 406, 368
- Wake, D. A., Collins, C. A., Nichol, R. C., Jones, L. R., & Burke, D. J. 2005, ApJ, 627, 186
- Wang, L., Yang, X., Shen, S., Mo, H. J., van den Bosch, F. C., Luo, W., Wang, Y., Lau, E. T., Wang, Q. D., Kang, X., & Li, R. 2014, MNRAS, 439, 611
- Wetzel, A. R., Tinker, J. L., & Conroy, C. 2012, MNRAS, 424, 232
- Whitaker, K. E., van Dokkum, P. G., Brammer, G., & Franx, M. 2012, ApJ, 754, L29
- Yang, X., Mo, H. J., van den Bosch, F. C., & Jing, Y. P. 2005, MNRAS, 356, 1293
- Yang, X., Mo, H. J., van den Bosch, F. C., Pasquali, A., Li, C., & Barden, M. 2007, ApJ, 671, 153

This page intentionally left blank.